Impedance spectroscopy of TiO_2 thin films showing resistive switching

Doo Seok Jeong,[a] Herbert Schroeder, and Rainer Waser
Institut für Festkörperforschung and Center of Nanoelectronic Systems for Information Technology (CNI), Forschungszentrum Jülich, D 52425 Jülich, Germany

(Received 15 March 2006; accepted 27 June 2006; published online 24 August 2006)

Impedance characteristics of 27 nm thick anatase TiO_2 films showing bistable resistive switching were investigated in the frequency domain (100 Hz–10 MHz) in various resistance states, a fresh state (before electroforming), a high resistive state (HRS), and a low resistive state (LRS). dc conductance in the film becomes dominent in HRS and LRS and the capacitances in the various states are almost identical. Numerical calculations using finite element analysis were performed for the localized filament and homogeneous model, whose results suggest that the filament model is consistent with the experimental results. © *2006 American Institute of Physics*.
[DOI: 10.1063/1.2336621]

Resistive switching of transition metal oxide (TMO) materials including TiO_2, (Ref. 1 and 2) and NiO (Ref. 3) as well as perovskite-type oxides including $SrZrO_3$,[4] $Pb(Zr_x,Ti_{1-x})O_3$,[5] and $Pr_{0.7}Ca_{0.3}MnO_3$ (Ref. 6) is a very attractive subject of research. These materials show characteristic bistable resistance states, a high resistive state (HRS) and a low resistive state (LRS).

Despite the fact that resistive switching in TMOs has been studied for decades,[7,8] the working mechanism is still not clearly identified. However, owing to the advancement of microscopic observation technologies, e.g., scanning tunneling microscopy and atomic force microscopy (AFM), indications for the generation and rupture of local conduction pathways as the mechanism of the resistive switching have been found,[9,10] which support the filament model.[11,12] Impedance spectroscopy is a very useful method to define the arrangements of electrical components in dielectric films, including resistance, inductance, and capacitance as well as a dielectric dispersion in a frequency domain.[13,14]

In this study, sample test (ST) capacitors consisting of $Pt/TiO_2/Pt$ and short-circuit standard (SCS) capacitors excluding the TiO_2 thin film were fabricated and the impedance in the frequency domain (100 Hz–10 MHz) for the three different resistive states fresh state (FS) was investigated (before electroforming) HRS, and LRS). In order to obtain the intrinsic impedance, one has to calibrate the measured impedance spectra of the ST by removing the parasitic impedance mainly due to electrodes and wiring, which can be measured from the SCS capacitors. For further insight into the switching mechanism, the impedance spectra were simulated using finite element analysis (FEA) for two switching mechanisms, the filament model and the homogeneous model.[15]

The ST capacitors were fabricated by reactive sputtering of a 27 nm thick blanket TiO_2 film grown on a platinized Si wafer at room temperature. The structure of the grown film was nanocrystalline anatase in the as-deposited state, as confirmed by x-ray diffraction and transmission electron microscopy. The thickness of the film was measured by x-ray fluorescence and its stoichiometry (Ti:O) was determined as (1:2) by Rutherford backscattering spectroscopy. Finally, 70 nm thick circular top electrodes (Pt) with three different areas (0.015, 0.028, and 0.066 mm^2) were sputtered on the TiO_2 film at room temperature using a shadow mask. The SCS capacitors were simply formed on a platinized Si wafer by depositing identical top electrodes. Resistive switching measurements for the ST capacitors were performed using dc voltage-sweep mode of an HP4155A semiconductor parameter analyzer. The impedance spectra of the ST and SCS capacitors in the frequency domain (100 Hz–10 MHz) were measured at zero dc bias with a voltage oscillation amplitude of 50 mV using an HP4194A impedance analyzer. Figure 1 shows measured current versus dc voltage curves of the ST capacitor with an area of 0.015 mm^2 at different resistance states, representing a typical unipolar switching behavior, unlike the bipolar switching of perovskite-type oxides.[4–6] In order to prevent permanent dielectric breakdown during switching from HRS to LRS, curves (a) and (e), a current compliance of 7 mA was set. The current for switching from LRS to HRS, curves (c) and (d), was around 30 mA. The current in HRS increases along the curve (a) or (e) with increasing positive or negative dc voltage. After switching from HRS to LRS the current is limited by the current compliance and reduced to zero along the dashed line (b) or (f). Then, independent from the polarity of the applied voltage, switching to HRS can occur along the curve (c) or (d).

The ST capacitors show reproducible resistive switching regardless of the area of the top electrode. The measured conductance in the FS is proportional to the area of the top

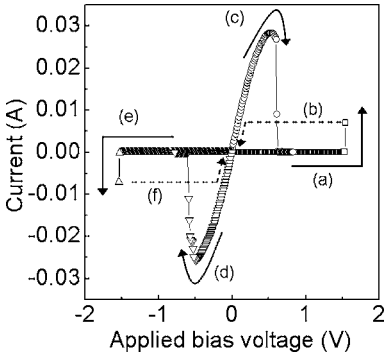

FIG. 1. Typical current vs dc voltage curves for unipolar resistive switching for a Pt/27 nm thick TiO_2/Pt capacitor with a capacitor area of 0.015 mm^2.

[a]Electronic mail: d.s.jeong@fz-juelich.de

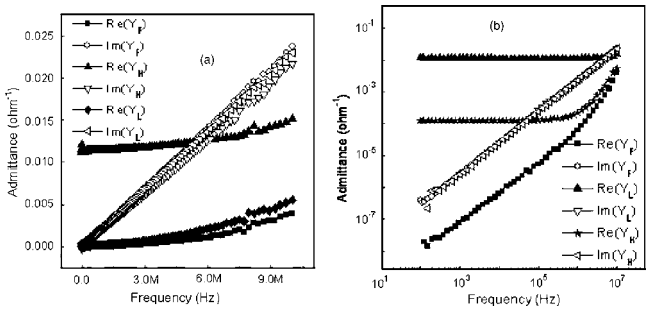

FIG. 2. Frequency dependence of the real (closed symbols) and imaginary (open symbols) parts of the intrinsic admittance (Y_c) of TiO_2 at the various resistance states, FS (subscript FS), HRS (subscript HRS), and LRS (subscript LRS) on (a) linear and (b) log scales.

electrode, but for HRS and LRS this trend is not observed (unreported results). In contrast, the measured resistances show large variations, so that it is rather improbable that the entire volume or area below the top electrode contributes to the resistive switching in a homogeneous manner, which favors the assumption of more local resistance changes responsible for switching as described by the filament model.

Regarding the electrode impedance Z_s due to the resistive and inductive components of the electrode, as being in series with the intrinsic TiO_2 impedance Z_c gives the impedance of ST, $Z_{ST}=Z_s+Z_c$. Because $Z_{SCS}=Z_s$, Z_c is simply expressed by $Z_c=Z_{ST}-Z_{SCS}$. A proper equivalent circuit of the filament model is an element with parallel connection of a capacitance and ac and dc conductances. The equivalent circuit of the homogeneous model is different, namely, a series connection of at least two such elements representing a conducting homogeneous bulk and a less conducting, but switchable thin region covering the whole capacitor area homogeneously, e.g., interface regions (for illustration, see Fig. 3). The equivalent circuit of the filament model can be expressed in terms of admittance $Y_c=Z_c^{-1}$, as

$$Y_c = j2\pi f C(f) + 1/R_L, \tag{1}$$

where

$$C(f) = C'(f) - jC''(f) = [1 + \chi'(f) - j\chi''(f)]\varepsilon_0 A/t, \tag{2}$$

where f, R_L, ε_0, A, and t denote the frequency, the resistance due to dc leakage current in the dielectric, the permittivity of vacuum, and the area and thickness of the dielectric, respectively. $C'(f)$, $C''(f)$, $\chi'(f)$, and $\chi''(f)$ are the real and imaginary parts of the complex capacitance and susceptibility, respectively. $C''(f)$, attributed to dielectric damping, makes the ac conductance distinguishable from the dc conductance due to leakage current. .

Figures 2(a) and 2(b) show the real and imaginary parts of the calibrated intrinsic admittance of TiO_2 (in FS, HRS, and LRS, respectively) on linear and log scales, respectively. For the case of FS, R_L^{-1} can be neglected because the contribution of the dc conductance to the admittance seems to be negligible. In Fig. 2(b) the real and imaginary parts of the complex admittance in FS, $\mathrm{Re}(Y_{FS})$ and $\mathrm{Im}(Y_{FS})$ show a power law behavior up to ~2 MHz, satisfying the Curie–von Schweidler relaxation law where both $\chi'(f)$ and $\chi''(f)$ are given by a power law, f^{n-1}, with n slightly less than unity.[16,17] Therefore, their ratio becomes constant, $\chi''(f)/[1+\chi'(f)] \approx \chi''(f)/\chi'(f) = \cot(n\pi/2)$.[18] The exponent n is found to be 0.975, for which a dielectric dispersion in the given frequency domain is negligible. Therefore, the dielectric constant is 75.7, independent from frequency, and both $C'(f)$ and $C''(f)$ can be regarded as constants in the given domain. The dielectric constant is much higher than other anatase TiO_2 reported elsewhere, which may be attributed to the nanograin structure; however, the concrete reason is still unclear. The dielectric constant of 80 nm thick TiO_2 is also consistent with the value reported in this letter (unreported result). Furthermore, Fig. 2 shows that the different resistance states have negligible influence on $\mathrm{Im}(Y_c)$; the capacitance $C'(f)$ is almost constant regardless of the resistive states.

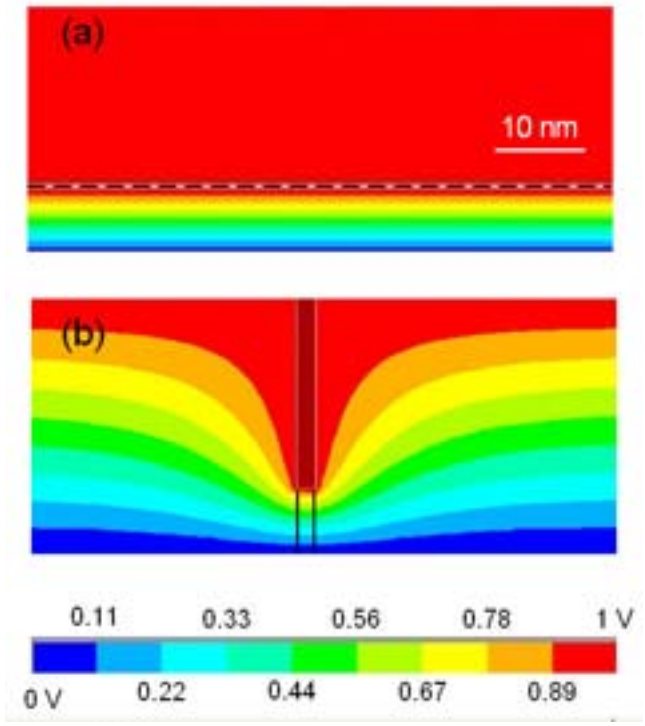

FIG. 3. (Color online) Voltage distribution (application of 1 V on the top electrode) in dielectric films in HRS for (a) the homogeneous model and (b) the filament model obtained by FEA.

It is also found that $\mathrm{Re}(Y_c)$ of HRS is almost constant until the ac conductance becomes dominent, which is consistent with the assumption of a parallel connection between the ac and dc conductances satisfying Eq. (1). For the case of LRS the dc conductance is high enough to hide the ac conductance completely in the whole frequency domain. These observations can serve as critical clues to identify a mechanism of the resistive switching, e.g., either a homogeneous model or the filament model.

For a comparison of the impedance spectra between the two suggested mechanisms, numerical calculations of the impedance spectra for the 27 nm thick film were performed using FEA with varying distributions of the charge carriers (electrons) in the dielectric film, (i) a very low and uniform carrier density corresponding to FS, (ii) uniformly distributed carriers in conducting and insulating regions, which are separated by a virtual cathode, corresponding to the homogeneous model with interface regions, and (iii) highly localized high density of carriers in a filament. The numerically calculated voltage distributions in HRS for the cases (ii) and (iii) are shown in Figs. 3(a) and 3(b). The voltage distribution of (i) is omitted as a separate figure because the result is

obvious and identical to that at the left and right edges in Fig. 3(b). The dashed line of Fig. 3(a) designates the virtual cathode dividing the dielectric into a conducting (upper) and insulating (lower) region. The hatched area in Fig. 3(b) designates a ruptured, highly conducting filament. For the FEA calculation of the homogeneous model shown in Fig. 3(a), the thicknesses of the conducting and insulating phases in HRS are assumed to be 20 and 7 nm, respectively. Using the resistances in LRS and HRS in Fig. 2, 83 and 8300 Ω, respectively, and the corresponding capacitor area of 0.015 mm^2, the resistivities of the conducting and insulating regions are 4.6×10^3 and 1.8×10^6 Ω cm, respectively. For the FEA calculation of the filament model shown in Fig. 3(b) the width of the conducting filament is set to 2 nm. In HRS the filament is assumed to be destroyed on a length of 7 nm so that only 20 nm still have a high conductivity. Obtaining the resistance of a highly conducting filament from conductive AFM measurements,[19] the resistivity of the 2 nm wide filament is calculated to be 5.2×10^{-3} Ω cm. To fit the resistance in LRS in Fig. 2, about 5200 filaments must be present, resulting in a density of 3.45×10^7 cm^{-2}. Fitting HRS with also this density gives the resistivity of the broken filament part, which is 1.93 Ω cm. The resistivity of the insulating phase is 6.63×10^9 Ω cm calculated from the resistance of the FS-TiO_2, measured by applying dc voltage. It should be pointed out that these filament resistivities are only order of magnitude estimations because the resistances in HRS and LRS hardly scale with the electrode area, namely, fitting the resistances of the other capacitors with a different top electrode area gives different filament densities. In addition, the nature of the spatial and conductivity distributions of filaments still leaves many open questions. In the present letter, the conductivity distribution is not taken into account since the distribution would not influence the simulation results. The conduction behavior attributed to localized conduction paths hardly affects the bulk dielectric behavior of TiO_2 [no effect on $\mathrm{Im}(Y_c)$] as well as the frequency dispersion of $\mathrm{Re}(Y_c)$.

The impedance spectra for all three cases were calculated with the parameters mentioned above and are shown in Figs. 4. It can be noted that the calculations for the homogeneous model, case (ii), give rise to great changes of the complex admittance, which is in disagreement with the experimental impedance spectra. On the other hand, the impedance spectra of the filament model are in much better agreement with the experimental data.

In summary, capacitors of ($Pt/TiO_2/Pt$) were fabricated and resistive switching and impedance measurements were performed. In FS, TiO_2 shows the Curie–von Schweidler relaxation law, and in HRS and LRS, it is found that TiO_2 includes a dc conductance, depending on the resistance state $\mathrm{Im}(Y_c)$ of TiO_2 does not show significant variations with the varying resistive states, which plays a key role in the determination of an appropriate mechanism for resistive switching. From the simulated $\mathrm{Im}(Y_c)$ behavior in the frequency domain for the filament and homogeneous model, it could be noticed that the filament model is in better agreement with the experimental results.

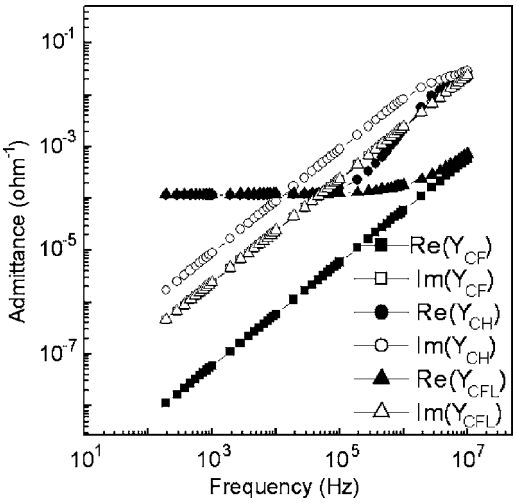

FIG. 4. Numerically calculated impedance spectra described in terms of the real (closed symbols) and imaginary (open symbols) parts of the complex admittance (Y) of FS excluding a good conducting phase (Y_{CF}), the homogeneous model (Y_{CH}), and the filament model (Y_{CFL}), respectively.

One of the authors (D.S.J.) would like to thank the Deutscher Akademischer Austausch Dienst for the scholarship supporting his research at the Forschungszentrum Jülich GmbH and C. S. Hwang of Seoul National University, South Korea, for fruitful discussion and advice. The authors also thank X. Guo for carefully reading this letter.

[1] F. Argall, Solid-State Electron. **11**, 535 (1968).
[2] B. J. Choi, D. S. Jeong, S. K. Kim, C. Rohde, S. Choi, J. H. Oh, H. J. Kim, C. S. Hwang, R. Waser, B. Reichenberg, and S. Tiedke, J. Appl. Phys. **98**, 033715 (2005).
[3] J. F. Gibbons and W. E. Beadle, Solid-State Electron. **7**, 785 (1964).
[4] A. Beck, J. G. Bednorz, Ch. Geber, C. Rossel, and D. Widmer, Appl. Phys. Lett. **77**, 139 (2000).
[5] J. R. Contreras, H. Kohlstedt, U. Poppe, R. Waser, C. Buchal, and N. A. Pertsev, Appl. Phys. Lett. **83**, 4595 (2003).
[6] A. Sawa, T. Fujii, M. Kawasaki, and Y. Tokura, Appl. Phys. Lett. **85**, 4073 (2004).
[7] G. Dearnaley, A. M. Stoneham, and D. V. Morgan, Rep. Prog. Phys. **33**, 1129 (1970).
[8] N. F. Mott, Rev. Mod. Phys. **40**, 677 (1968).
[9] K. Szot, W. Speier, R. Carius, U. Zastrow, and W. Beyer, Phys. Rev. Lett. **88**, 75508 (2002).
[10] O. Kurnosikov, F. C. de Nooij, P. LeClair, J. T. Kohlhepp, B. Koopmans, H. J. M. Swagten, and W. J. M. de Jonge, Phys. Rev. B **64**, 153407 (2001).
[11] S. Gravano and R. D. Gould, Int. J. Electron. **73**, 315 (1992).
[12] A. K. Ray and C. A. Hogarth, Thin Solid Films **127**, 69 (1985).
[13] J. D. Baniecki, R. B. Laibowitz, T. M. Shaw, P. R. Duncombe, D. A. Neumayer, D. E. Kotecki, H. Shen, and Q. Y. Ma, Appl. Phys. Lett. **72**, 498 (1998).
[14] R. Waser, Integr. Ferroelectr. **15**, 39 (1997).
[15] K. Szot, W. Speier, and W. Eberhardt, Appl. Phys. Lett. **60**, 1190 (1992).
[16] J. Curie, Ann. Chim. Phys. **18**, 203 (1889).
[17] E. von Schweidler, Ann. Phys. **24**, 711 (1907).
[18] A. K. Jonscher, J. Phys. D **32**, R57 (1999).
[19] D. S. Jeong, K. Szot, H. Schroeder, and R. Waser (unpublished).